



Surface plasmon resonance biosensor-based dual-core photonic crystal fiber: design and analysis

A. Arunya Revathi¹ · D. Rajeswari¹

Received: 22 September 2019 / Accepted: 13 February 2020 / Published online: 21 March 2020
© The Optical Society of India 2020

Abstract A finite element analysis of biosensor-based dual-core photonic crystal fiber is conducted using surface plasmon resonance model and is presented in this article. Calculated wavelength sensitivity of the sensor is around 10,000 nm/RIU and 5000 nm/RIU for *x*-polarization and *y*-polarization, respectively, when analyte refractive index is 1.34. Amplitude sensitivity for *x*-polarization and *y*-polarization is 334 RIU⁻¹ and 394 RIU⁻¹, respectively. Resolution for both polarizations is 2×10^{-5} RIU. Consequently, the proposed biosensor can detect the low-refractive-index biochemical analyte at different wavelengths.

Keywords Photonic crystal fiber (PCF) · Surface plasmon resonance (SPR) · Biosensor · Finite element method (FEM)

Introduction

In recent years, the immense development of a new type of photonic crystal fiber (PCF) with an array of air holes along the propagation direction has more attractive research work going worldwide. PCFs can be divided into a two broad classes according to whether they use index guiding (guides light by total internal reflection (TIR) between a high-refractive-index core and a low-refractive-index cladding region) or band gaps (guides light by the photonic band gap in a low-refractive-index core region) for optical

confinement. PCF sensors have more attractive applications like optical sensors [1, 2], surface plasmon resonance (SPR) sensors [3–8], biosensor [9], humidity sensor [10], optical amplifier [11], temperature sensor [12] and pressure sensor [13]. PCF sensors are now a newfangled subject of field study due to the various advantages offered by PCFs such as high confinement compare to conventional optical fiber, flexible design and limit the distortion [14]. The theoretical concept of surface plasmons was introduced by Ritchie [15]. Using a related concept, Otto [16] and Kretschmann [17] have established sensing-based techniques. Surface plasmon is a near-field electromagnetic interaction formed on the surface of the metal and dielectric. When light waves are incident to the metal and the dielectric interface, a collective oscillation of free electrons on the surface of the metal occurs, and the electromagnetic waves couple to the free electron; then, surface plasmon forms. For example, if the frequency of electron oscillation and the frequency of the incident wave are consistent, it will produce resonance. Sensor with gold-coated core has been developed in optical fiber, which excites surface plasmon [18]. Resonance peak will be shifted at phase matching condition. Particular wavelength is called phase matching wavelength when phase matching occurs it. Loss spectrum of SPP and fundamental mode will match at phase matching wavelength. This is the basic condition for sensing. In recent times, many researchers have to design photonic crystal fiber SPR sensors, because these sensors offers high sensitivity, structural reduction, robust, fabrication flexibility and lower cost [19]. Two-dimensional photonic lattices of gold and silver nanowires were developed and fabricated [20].

In this paper, surface plasmon resonance photonic crystal fiber biosensor is proposed. Gold-coated air hole is placed in the center of PCF. Gold is acted as a sensing

✉ D. Rajeswari
drajeswari1992@gmail.com

¹ Department of Electrical and Electronics Engineering,
Alagappa Chettiar Government College of Engineering and
Technology, Karaikudi, Tamilnadu, India

layer. Next to the center air hole is filled with unknown analyte. This analyte is reacting with the surface plasmon. This leads to phase matching condition. Gold is the suitable plasmonic material compared to silver, because it has high resonance peak shift [21]. PCF with boundary condition is simulated using finite element method.

Structure and theory

The simplified graphic representation of the designed photonic crystal fiber is shown in Fig. 1. The diameter of small air holes (d_1) and large air holes (d_2) are 1 μm and 1.6 μm , respectively. Pitch can be fixed with the value of 2 μm .

Blue shaded air hole is filled with gold nanowire. Cladding is filled with the material silica. Red shaded air hole is filled with analyte. Other holes are filled with air. Electric field is applied to the PCF, i.e., light is pass through the fiber; metal–dielectric interface leads to surface plasmon generation. Phase matching occurs means resonance peak will be shifted. Fundamental mode and SPP mode has high-loss spectrum. Due to this phase matching condition, maximum loss occurs at particular wavelength [22].

Coupling between SPP and core modes is represented by coupling theory [23]:

$$\frac{dE_1}{dz} = i\beta_1 E_1 + ikE_2 \quad (1)$$

$$\frac{dE_2}{dz} = ikE_1 + i\beta_2 E_2 \quad (2)$$

Here, E_1 and E_2 are mode fields of the core guided mode and plasmon mode; β_1 and β_2 are propagation constants of guided mode and plasmon mode, respectively. Direction of the propagation is along z direction. Strength of coupling is denoted by k . Difference in propagation constant of core and plasmonic mode is zero when phase matching occurs. To reduce the energy loss, PML (perfectly matched layer) is applied to the structure.

Pure silica is used as background material, and wavelength-dependent Sellmeier equation of the material is [24]

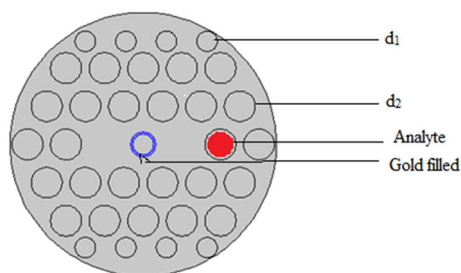


Fig. 1 Simplified picture representation of the designed PCF structure

$$n(\lambda)^2 = 1 + \frac{A_1 \lambda^2}{\lambda^2 - \lambda_1^2} + \frac{A_2 \lambda^2}{\lambda^2 - \lambda_2^2} + \frac{A_3 \lambda^2}{\lambda^2 - \lambda_3^2} \quad (3)$$

Here, $A_1 = 0.6961663$, $A_2 = 0.4079426$, $A_3 = 0.897479$, $\lambda_1 = 0.068404$, $\lambda_2 = 0.1162414$ and $\lambda_3 = 9.896161$ are the coefficients for the material, and operating wavelength is λ . Similarly, the material dispersion of gold is also categorized by the Drude–Lorentz model [22] and could be stated as:

$$\varepsilon(\omega) = \varepsilon_\infty - \frac{w_p^2}{w^2 + i\Gamma_p w} - \frac{f_1 w_1^2}{w^2 - w_1^2 - i\Gamma_1 w} \quad (4)$$

Here, w is angular frequency. At high frequency, the permittivity of gold is ε_∞ . Plasma frequency and damping frequency by Drude model are w_p and Γ_p . f_1 is the weighting factor. Lorentz oscillator has the frequency is w_1 , and spectral width is Γ_1 . Table 1 lists the parameters and values of gold dispersion equation.

The wavelength sensitivity is calculated by using wavelength interrogation method [25].

$$S(\lambda) = \frac{\partial \lambda_{\text{peak}}}{\partial n_a} \quad (\text{nm/RIU}) \quad (5)$$

Here, $\partial \lambda_{\text{peak}}$ depends on the analyte refractive index. At resonance condition, loss peaks are high. Different loss peaks are occurring for different filled analyte refractive indices. ∂n_a is the analyte refractive index difference. Amplitude sensitivity of the sensor is calculated by using the following equation. This technique of calculation is called amplitude interrogation technique [26].

$$S_A(\lambda) = -\frac{1}{\alpha(\lambda, n_a)} \left(\frac{\partial \alpha(\lambda, n_a)}{\partial n_a} \right) \quad (\text{RIU}^{-1}) \quad (6)$$

Here, $\alpha(\lambda, n_a)$ is the confinement loss of the fundamental core mode and depends on wavelength. $\partial \alpha(\lambda, n_a)$ is the difference of confinement loss.

The following equation represents the resolution (R) of sensor [27, 28]

$$R = \frac{\partial n_a \cdot \partial \lambda_{\text{min}}}{\partial \lambda_{\text{peak}}} \quad (7)$$

Dual-core PCF-based SPR sensor is proposed in this paper. Finite element method (FEM) is used to study the proposed sensor. Perfectly matched layer (PML) with PCF structure is used to avoid the energy loss. Analyte refractive index is taken from 1.33 to 1.35. In addition, thickness

Table 1 Parameters and their values of gold dispersion equation

ε_∞	$w_p/2\pi$	$\Gamma_p/2\pi$	f_1	$w_1/2\pi$	$\Gamma_1/2\pi$
5.9673	2113.6	15.92	1.09	650.07	104.86

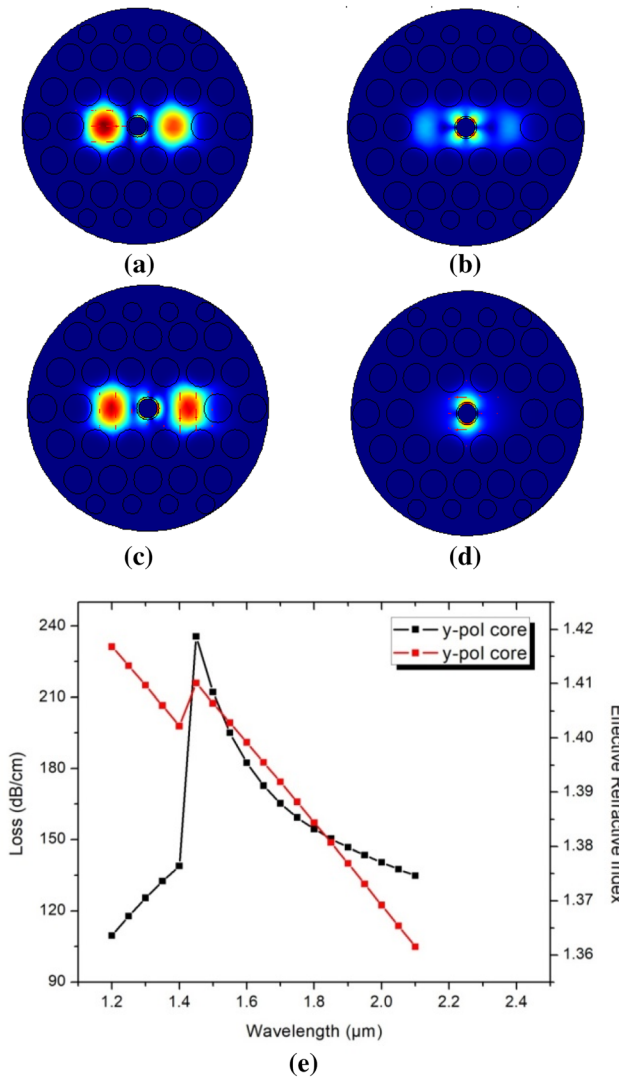


Fig. 2 Optical field distribution of the proposed dual-core PCF **a** *x*-polarized and **c** *y*-polarized fundamental mode, **b** *x*-polarized, **d** *y*-polarized SPP mode and **e** confinement loss for *y*-polarized mode at analyte RI of 1.33 with $t_g = 0.2 \mu\text{m}$

of gold layer is varied for obtaining the better performance of the sensor.

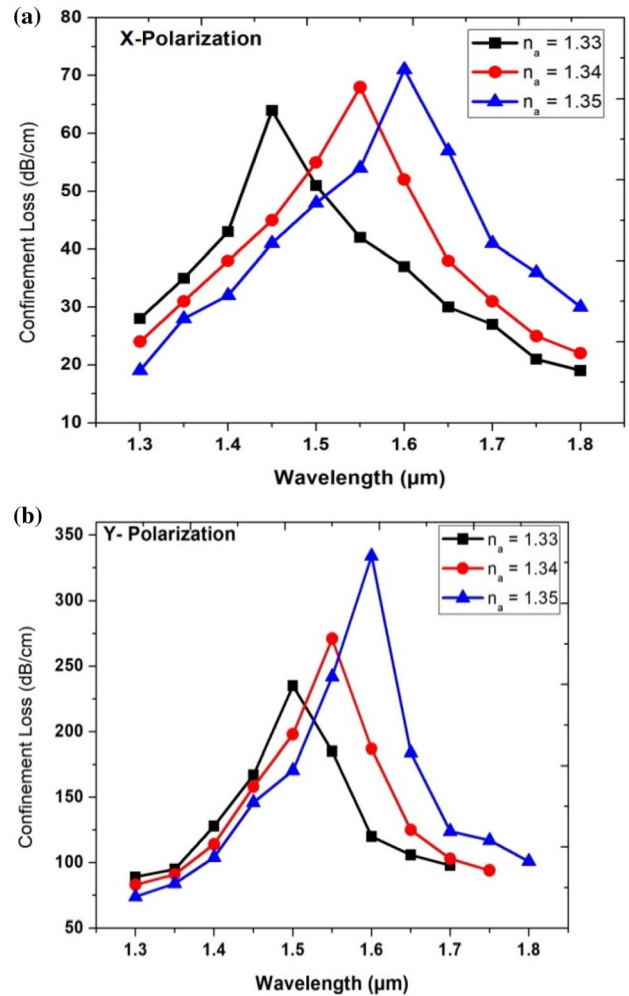


Fig. 3 Loss spectrum of **a** *x*-polarized, **b** *y*-polarized modes with $t_g = 0.2 \mu\text{m}$

Numerical Results and Discussion

Figure 2 shows the optical field distribution of the proposed sensor. It is clear that the loss of *y*-polarized mode is higher so that maximum energy loss arises at *y*-polarization

Table 2 Performance analysis comparison of the proposed sensor with existing sensors

PCF sensor	Wavelength sensitivity (nm/RIU)	Maximum amplitude sensitivity (RIU ⁻¹)	Peak loss (dB/cm)	Sensor resolution (wavelength inte.) (RIU)
Ref. [29]	1000	118	19.9	2.4×10^{-5}
Ref. [30]	2000	80	2500	5×10^{-5}
Ref. [31]	2200	266	160	3.75×10^{-5}
Ref. [32]	9000	318	700.05	1.11×10^{-5}
Proposed	10,000 <i>x</i> - 5000 <i>y</i> -	334 <i>x</i> - 394 <i>y</i> -	72 <i>x</i> - 337 <i>y</i> -	2×10^{-5}

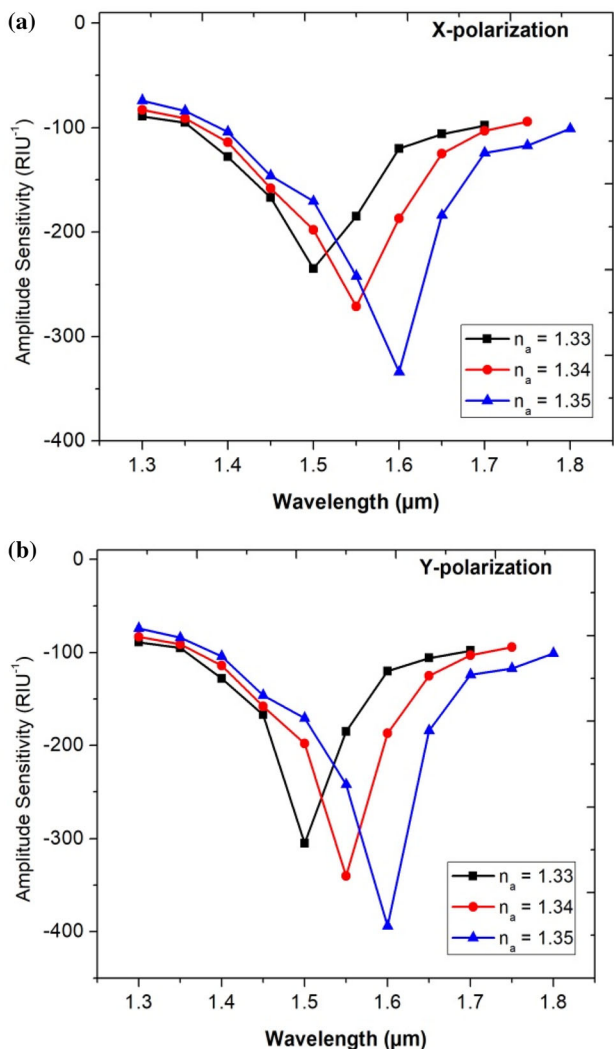


Fig. 4 Amplitude sensitivity of **a** *x*-polarized, **b** *y*-polarized modes with $t_g = 0.2 \mu\text{m}$

compared to *x*-polarization and it is evident for maximum energy transferred to cladding region. One more is that *x*-polarization takes place when more energy is accumulated in core region. Figure 2e demonstrates the real part of effective index of core mode, and their losses are depend on wavelength. Confinement loss is calculated by using the formulae as stated in [27].

$$C_L = 8.686 \times \left(\frac{2\pi}{\lambda} \right) \cdot \text{Im}(n_{\text{eff}}) \times 10^4 \text{ (dB/cm)} \quad (8)$$

Here, imaginary part of effective refractive index is $\text{Im}(n_{\text{eff}})$ and $\left(\frac{2\pi}{\lambda} \right) = k_0$ is the free space wave number. Two regions will act as a core due to the RI variation between the center and surrounded cladding (Table 2).

For *x*-polarization, the maximum loss occurs at wavelength of 1.45 μm , 1.55 μm and 1.6 μm for the analyte

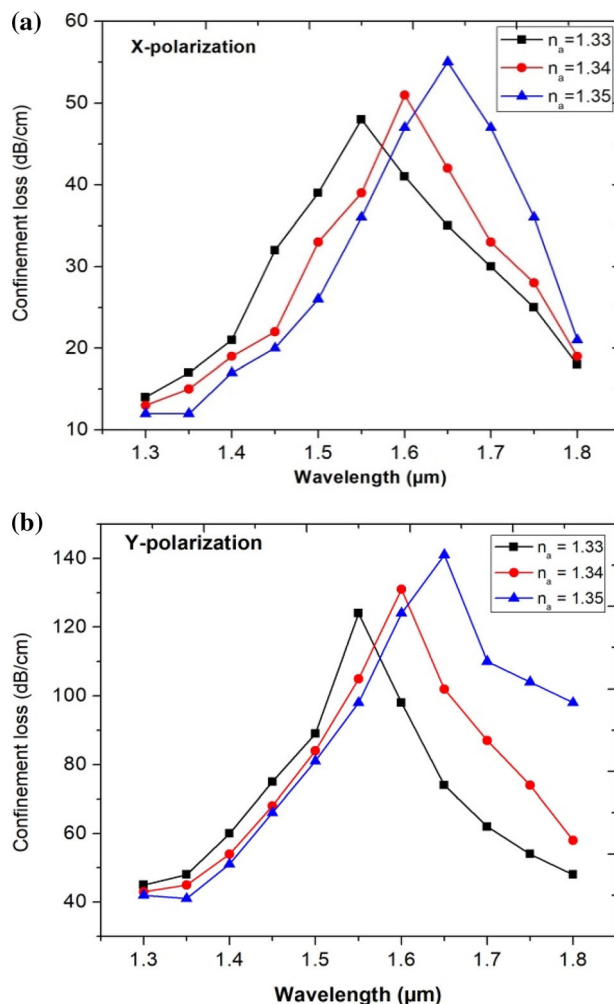


Fig. 5 Loss curve of **a** *x*-polarized, **b** *y*-polarized modes with $t_g = 0.3 \mu\text{m}$

refractive index of 1.33, 1.34 and 1.35, respectively. Confinement loss is high at 1.5 μm , 1.55 μm and 1.6 μm for the RI of analyte of 1.33, 1.34 and 1.35, respectively, for *y*-polarization. Wavelength sensitivity is 10,000 nm/RIU and 5000 nm/RIU for the RI of analyte is 1.33 and 1.34, respectively, for *x*-polarization. Wavelength sensitivity is 5000 nm/RIU and 5000 nm/RIU for the corresponding analyte RI of 1.33 and 1.34, respectively, for *y*-polarization (Fig. 3).

In Fig. 4, the amplitude sensitivity is 235 RIU^{-1} , 271 RIU^{-1} and 334 RIU^{-1} for analyte RI of 1.33, 1.34 and 1.35, respectively, for *x*-polarization. For analyte RI of 1.33, 1.34 and 1.35, amplitude sensitivity is 305 RIU^{-1} , 340 RIU^{-1} and 394 RIU^{-1} , respectively, for *y*-polarization. The technique to calculate amplitude sensitivity is called amplitude interrogation technique (Fig. 5).

The proposed biosensor has reasonable resolution with good sensitivity.

Conclusion

SPR biosensor-based dual-core photonic crystal fiber (DC-PCF) has been investigated in this paper. Investigation of the sensor is done by using finite element method. From the simulation result, wavelength sensitivity is obtained around 10,000 nm/RIU and 5000 nm/RIU with analyte refractive index of 1.34 for x -polarization and y -polarization. 334 RIU⁻¹ and 394 RIU⁻¹ are the amplitude sensitivity for x -polarization and y -polarization, respectively. Resolution for both polarizations is 2×10^{-5} RIU. So, the proposed biosensor can detect the analyte of low refractive index at different wavelengths.

References

- M. Morshed, M. Imran Hassan, T.K. Roy, M.S. Uddin, S.M. Abdur Razzak, Microstructure core photonic crystal fiber gas sensing Applications. *Appl. Opt.* **54**(29), 8637 (2015)
- K. Ahmed, M. Morshed, Design and Numerical analysis of microstructure core octagonal photonic crystal fiber for sensing applications. *Sens. Bio-Sen. Res.* **7**, 1–6 (2016)
- J. Homola, Present and future of surface plasmon resonance biosensors. *Anal. Bioanal. Chem.* **377**, 528–539 (2003)
- R. Otupiri, E. Akowuah, S. Haxha, H. Ademgil, F. AbdelMalek, A. Aggoun, A novel birefringent photonic crystal fibre surface plasmon resonance biosensor. *IEEE Photon. J.* **6**, 1–11 (2014)
- J.G. Ortega-Mendoza, A. Padilla-Vivanco, C. Toxqui-Quitl, P. Zaca-Morán, D. Villegas-Hernández, F. Chávez, Optical fiber sensor based on localized surface plasmon resonance using silver nanoparticles photodeposited on the optical fiber end. *Sensors* **14**, 18701–18710 (2014)
- E.K. Akowuah, T. Gorman, H. Ademgil, S. Haxha, G.K. Robinson, J.V. Oliver, Numerical analysis of a photonic crystal fiber for biosensing applications. *IEEE J. Quantum Electron.* **48**, 1403–1410 (2012)
- A.A. Rifat, R. Ahmed, A.K. Yestisen, H. Butt, A. Sabouri, G.A. Mahdiraji, S.H. Yun, F.R. Adikan, Photonic crystal fiber based plasmonic sensors. *Sens. Actuators B Chem.* **243**, 311–325 (2017)
- M.R. Hasan, S. Akter, A.A. Rifat, S. Rana, K. Ahmed, R. Ahmed, D. Abbott, Spiral photonic crystal fiber based dual-polarized surface plasmon resonance biosensor. *IEEE Sens. J.* **18**(1), 133–140 (2018)
- A.A. Rifat et al., Surface Plasmon Resonance photonic crystal fiber biosensor: a practical approach. *IEEE Photon. Technol. Lett.* **27**(15), 1628–1631 (2015)
- M.Y. Mohd Noor et al., Optical humidity sensor based on air guided photonic crystal fiber. *Photonic Sens.* **2**(3), 277–282 (2012)
- S. Wabnitz, Broadband parametric amplification in photonic crystal fiber with two zero-dispersion wavelengths. *J. Lightwave Technol.* **24**(4), 1732–1738 (2006)
- Y. Yu et al., Some features of the photonic crystal fiber temperature sensor with liquid ethanol filling. *Opt. Express* **18**(15), 15383 (2010)
- H.Y. Fu et al., High pressure sensor based on photonic crystal fiber for downhole application. *Appl. Opt.* **49**(14), 2639 (2010)
- P. Russell, J. St, Photonic crystal fibers. *Science* **299**, 358–362 (2003)
- R.H. Ritchie, Plasma losses by fast electrons in thin films. *Phys. Rev.* **106**(5), 874–881 (1957)
- A. Otto, Excitation of nonradiative surface plasma waves in silver by the method of frustrated total reflection. *Z. Phys.* **216**, 398–410 (1968)
- E. Kretschmann, Radiative decay of non radiative surface plasmons excited by light. *Z. Naturforschung A* **23**(12), 2135–2136 (1968)
- R. Jorgenson, S. Yee, A fiber-optic chemical sensor based on surface plasmon resonance. *Sens. Actuators B Chem.* **12**, 213–220 (1993)
- B.D. Gupta, Surface plasmon resonance based fiber optic sensors, in *Reviews in Plasmonics 2010*, ed. by C. Geddes (Springer, Berlin, 2012), pp. 105–137
- M.A. Schmidt, L.P. Sempere, H.K. Tyagi, C.G. Poulton, P.S.J. Russell, Waveguiding and plasmon resonances in two dimensional photonic lattices of gold and silver nanowires. *Phys. Rev. B* **77**, 033417 (2008)
- P. Zhang, J. Yao, H. Cui, Y. Lu, A surface plasmon resonance sensor based on a multi-core photonic crystal fiber. *Optoelectron. Lett.* **9**, 342–345 (2013)
- L. Chen, W.G. Zhang, Z. Zhang, Y.J. Liu, J. Sieg, L.Y. Zhang, Design for a single-polarization photonic crystal fiber wavelength splitter based on hybrid-surface plasmon resonance. *IEEE Photonics J.* **21**, 1–9 (2014)
- P. Li, J.L. Zhao, Polarization-dependent coupling in gold filled dual-core photonic crystal fibers. *Opt. Express* **21**, 5232–5238 (2012)
- Q. Liu, S.G. Li, H. Li, J. Zi, W. Zhang, Z.K. Fan, G.W. An, Y.J. Bao, Broadband single-polarization photonic crystal fiber based on surface plasmon resonance for polarization filter. *Plasmonics* **10**, 1–9 (2015)
- C. Liu, L. Yang, W. Su, F. Wang, T. Sun, Q. Liu, H. Mu, P.K. Chu, Numerical analysis of a photonic crystal fiber based on a surface plasmon resonance sensor with an annular analyte channel. *Opt. Commun.* **382**, 162–166 (2017)
- M. Liu, X. Yang, P. Shum, H. Yuan, High-sensitivity birefringent and single-layer coating photonic crystal fiber biosensor based on surface plasmon resonance. *Appl. Opt.* **57**(8), 1883–1886 (2018)
- A. Rifat, G.A. Mahdiraji, D.M. Chow, Y.G. Shee, R. Ahmed, F.R.M. Adikan, Photonic crystal fiber-based surface plasmon resonance sensor with selective analyte channels and graphene-silver deposited core. *Sensors* **15**(5), 11499–11510 (2015)
- M. Hautakorpi, M. Mattinen, H. Ludvigsen, Surface-plasmon-resonance sensor based on three-hole microstructured optical fiber. *Opt. Express* **16**(12), 8427–8432 (2008)
- A.A. Rifat, G.A. Mahdiraji, Y.G. Shee, M.J. Shawon, F.M. Adikan, A novel photonic crystal fiber biosensor using surface plasmon resonance. *Procedia Eng.* **140**, 1–7 (2016)
- J.N. Dash, R. Jha, SPR biosensor based on polymer PCF coated with conducting metal oxide. *IEEE Photonics Technol. Lett.* **26**, 595–598 (2014)
- M.R. Hasan, S. Akter, A.A. Rifat, S. Rana, S. Ali, A highly sensitive gold-coated photonic crystal fiber biosensor based on surface plasmon resonance. *Photonics* **4**(1), 18 (2017)
- S. Chakma, M.A. Khalek, B.K. Paul, K. Ahmed, M.R. Hasan, A.N. Bahar, Gold-coated photonic crystal fiber biosensor based on surface plasmon resonance: design and analysis. *Sens. Bio-Sens. Res.* **18**, 7–12 (2018)

Publisher's Note Springer Nature remains neutral with regard to jurisdictional claims in published maps and institutional affiliations.